

Photophysical properties of ligand localized excited state in ruthenium(II) polypyridyl complexes: a combined effect of electron donor–acceptor ligand†

Sandeep Verma,^a Prasenjit Kar,^b Amitava Das^{*b} and Hirendra Nath Ghosh^{*a}

Received 18th February 2011, Accepted 8th July 2011

DOI: 10.1039/c1dt10266d

We have synthesized ruthenium(II) polypyridyl complexes (1) Ru(II)(bpy)₂(L₁), (2) Ru(II)(bpy)₂(L₂) and (3) Ru(II)(bpy)(L₁)(L₂), where bpy = 2,2'-bipyridyl, L₁ = 4-[2-(4'-methyl-2,2'-bipyridinyl-4-yl)viny]benzene-1,2-diol and L₂ = 4-(*N,N*-dimethylamino-phenyl)-(2,2'-bipyridine) and investigated the intra-ligand charge transfer (ILCT) and ligand–ligand charge transfer (LLCT) states by optical absorption and emission studies. Our studies show that the presence of electron donating –NMe₂ functionality in L₂ and electron withdrawing catechol fragment in L₁ ligands of complex 3 introduces low energy LLCT excited states to aboriginal MLCT states. The superimposed LLCT and MLCT state produces redshift and broadening in the optical absorption spectra of complex 3 in comparison to complexes 1 and 2. The emission quantum yield of complex 3 is observed to be extremely low in comparison to that of complex 1 and 2 at room temperature. This is attributed to quenching of the ³MLCT state by the low-emissive ³LLCT state. The emission due to ligand localized CT state (ILCT and LLCT) of complexes 2 and 3 is revealed at 77 K in the form of a new luminescence band which appeared in the 670–760 nm region. The LLCT excited state of complex 3 is populated either *via* direct photoexcitation in the LLCT absorption band (350–700 nm) or through internal conversion from the photoexcited ³MLCT (400–600 nm) states. The internal conversion rate is determined by quenching of the ³MLCT state in a time resolved emission study. The internal conversion to LLCT and ILCT excited states are observed to be as fast as ~200 ps and ~700 ps for complexes 3 and 2, respectively. The present study illustrates the photophysical property of the ligand localized excited state of newly synthesized heteroleptic ruthenium(II) polypyridyl complexes.

1. Introduction

Ruthenium(II) polypyridyl complexes have been studied extensively for their rich optoelectronic and redox properties.¹ Absorption and fluorescence spectra of these complexes are generally dominated by $d\pi_{\text{Ru(II)}} \rightarrow \pi^*_{\text{bpy/terpy}}$ -based transitions. Energies of the electronic transitions and the corresponding energy gap between $d\pi_{\text{Ru(II)}}$ -based highest occupied molecular orbitals (HOMO) and $\pi^*_{\text{bpy/terpy}}$ -based lowest unoccupied molecular orbitals (LUMO) can be tuned with appropriate substitution of the polypyridyl ligand (bpy or terpy) with suitable electron donor or acceptor functionalities.^{2,3} Recent advancements in the area of synthetic chemistry and vast number of literature reports draw an appropriate correlation between the structure and redox activity/spectral properties which helped in the design and synthesis of newer molecules with attractive spectral and redox behaviors. In this

regard, diimine ligands (bpy/terpy) substituted with electron-donating and electron-withdrawing groups, have drawn special attention as it introduces new ligand localized CT states to MLCT manifolds of metal–polypyridyl complexes.⁴ The optical response of such complexes are significantly modified by incorporating new intra-ligand charge-transfer (ILCT) or ligand–ligand charge-transfer (LLCT) transitions to aboriginal MLCT transitions.⁵ The appropriate selection of the substituent in diimine ligands of Ru(II) polypyridyl complexes may lower the energy of the ligand localized CT excited state in comparison to that of the $d\pi_{\text{Ru(II)}} \rightarrow \pi^*_{\text{bpy/terpy}}$ -based MLCT excited state. Thus, ligand localized CT states offer the possibility of a new deactivation channel of the photoexcited MLCT states, as these CT states could be populated by internal conversion from the original photoexcited MLCT states. Furthermore, a direct photoexcitation to a ligand localized CT band can produce such charge separated species instantly, without undergoing charge diffusion in excited states. The populated ligand localized CT excited states represents intramolecular charge separated states where electrons and counter positive charges (holes) reside on electron-acceptor and electron-donor ligands, respectively. In recent times, such a controlled intramolecular charge separation in metal–polypyridyl complexes

^aRadiation and Photo Chemistry Division, Bhabha Atomic Research Center, Mumbai, India. E-mail: hngosh@barc.gov.in

^bCentral Salt and Marine Chemicals Research Institute (CSIR), Bhavnagar, 364002, Gujarat, India. E-mail: amitava@csmcri.org

† Electronic supplementary information (ESI) available. See DOI: 10.1039/c1dt10266d

is desired for photovoltaic applications such as solar energy conversion,^{6,7} photocatalytic activity, electrochemiluminescence *etc.*⁸ In particular, the metal–polypyridyl complexes comprising ligand localized CT states were found to be useful in the field of dye sensitized solar cells (DSSC).^{7,9} So, the design and synthesis of ruthenium complexes exhibiting these properties are important in a way similar to optimization of photovoltaic devices based on such complexes.

Recent experimental as well as theoretical studies have described the role of ILCT and LLCT states in achieving a rapid intramolecular charge separation in metal–polypyridyl complexes which comprises of electron-donor and electron-acceptor ligands.^{10–15} In ruthenium–polypyridyl complexes, the singlet \rightarrow triplet excited state conversion (intersystem crossing process (ISC)) is accomplished in an ultrafast time scale (<100 fs).^{17,18} The inherent lower energetics¹³ of $^3\text{ILCT}$ or $^3\text{LLCT}$ states with respect to the $^3\text{MLCT}$ excited state, makes these ligand localized CT states active for photoluminescence in the near-IR region. The photoluminescence of such complexes were experimentally observed in the 650–850 nm region.¹⁹ The internal conversion from $^3\text{MLCT}$ to $^3\text{ILCT}$ or $^3\text{LLCT}$ states is reported as a dominant fast phase emission quenching of the $^3\text{MLCT}$ state in the sub ns time domain.^{20,21} Herein, the chemical nature of ancillary ligands defines the ILCT or LLCT character of final excited electronic states in Ru^{II} –polypyridyl complexes. For instance, Chou and co-workers¹⁶ have demonstrated a shift from $^3\text{ILCT}$ to $^3\text{LLCT}$ character in ligand localized CT states by the subsequent incorporation of electron withdrawing moieties in axial N-heterocyclic ligands. It suggests that ILCT or LLCT transitions are originating from specific substitution of N-donor ligands. So, in an effort to explore the ILCT and LLCT excited state, we have designed and synthesized a new series of ruthenium–polypyridyl complexes **1**, **2** and **3** (Scheme 1) by varying the chemical nature of the ancillary ligands. The ligand centered charge separation in complex **2** and **3** (after photoexcitation) is expected from the facile electron donor character of *N,N*-dimethylaniline (ph-NMe₂) moiety directly attached to the bpy fragment of L₂ ligand. Earlier, Zhang and co-workers²² have reported $^3\text{ILCT}$ states in a dimethylamino- α -styryl substituted Ru^{II} –diimine complex which is structurally related to complex **2** in this study. Moreover, in the case of complex **3**, the ligand centered charge separated excited states which are produced by the electron donor L₂ ligand can be stabilized by the low lying π^* (LUMO) level of the π -conjugated bipyridyl (bpy-CH=CH-) moiety and

the electron withdrawing nature of the catechol moiety of the L₁ ligand. Therefore, it will be interesting to study the photophysical property of complex **2** and complex **3** to identify the ligand localized CT states. In this present study, the ligand localized CT excited states (ILCT and LLCT states) are explored by carrying out comparative optical absorption and emission studies of complexes **1**, **2** and **3** under different ambient conditions such as aerated *vs.* de-aerated, protonated *vs.* de-protonated (at different pH) and ambient *vs.* low temperature. We have also carried out the time resolved emission measurements (using the time correlated single photon counting-TCSPC technique) to explore the $^3\text{MLCT} \rightarrow ^3\text{ILCT}$ or $^3\text{LLCT}$ internal conversion process. Our studies indicate strong LLCT behaviour of complex **3** in addition to weak ILCT behavior of complex **2**.

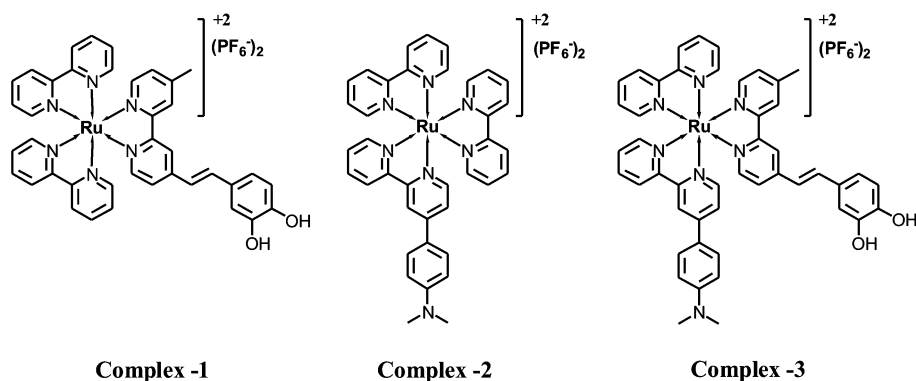
2. Experimental section

a) Materials

$\text{RuCl}_3 \cdot x\text{H}_2\text{O}$, 2,2'-bipyridyl, 3,4-dimethoxy benzaldehyde, acetaldehyde and 4-(*N,N*-dimethylamino) benzaldehyde were procured from Sigma-Aldrich and were used as received. Pyridine and ethanol, used as solvent, were dried and distilled prior to use. Nanopure water (Barnsted System, USA) is used for making aqueous solutions. All other reagents were of AR grade and procured from S.D. Fine Chemicals (India). HPLC grade acetonitrile (E. Mark, Bombay, India) is used for all spectrophotometric studies. Solvents were degassed thoroughly with dinitrogen gas (IOLAR grade purity) before use in the preparation of all standard solutions. 4-(*N,N'*-dimethylamino-phenyl)-propanal (**A**), pyridacyl pyridinium iodide salt (**B**), 4-(2,2'-bipyridinyl-4-yl)vinyl-benzene-1,2-diol (L₁), complexes **1** and **1**·Me₂ (**SI**) were synthesized following a previously reported procedure.^{23a,b}

b) Analytical methods

Microanalyses (C, H, N) were performed using a Perkin–Elmer 4100 elemental analyzer. FTIR spectra were recorded either as KBr pellets or as acetonitrile solutions in a cell fitted with a KBr window, using a Perkin–Elmer Spectra GX 2000 spectrometer. ¹H NMR spectra were recorded on a Bruker 200 MHz FT NMR (model: Avance-DPX 200) using CD₃CN and CD₃OD as the solvents and tetramethylsilane (TMS) as an internal standard; ESI MS measurements were carried out on a Waters QToF-Micro



Scheme 1 Molecular structure of complexes **1**, **2** and **3**.

instrument. Electronic spectra were recorded with a Shimadzu UV-3101 PC spectrophotometer; while steady state luminescence spectra were recorded using a Perkin–Elmer LS 50B luminescence spectrofluorimeter fitted with a red-sensitive photomultiplier. Electrochemical experiments were performed on a CH-660A electrochemical instrument with a conventional three-electrode cell assembly. A saturated Ag/AgCl reference and a platinum working electrode were used for all measurements. Ferrocene was added at the end of each measurement of the cyclic voltametric experiment as an internal standard.

c) Synthesis

(i) **4-(*N,N*-dimethylamino-phenyl)-propanal (A)**. 4-*N,N*-dimethylamino benzaldehyde (16.6 g) and acetaldehyde (5.6 mL) were dissolved in 40 mL of ethanol (95%). The mixture was cooled to 0 °C and to this 36 mL of 28% NaOH solution was added slowly then the solution was stirred vigorously and the temperature of the reaction mixture was maintained under 10 °C (15 min). After stirring further for 30 min at room temperature, 200 mL of water was added and the desired compound was extracted three times with 50 mL of ether. Then the ether layers were collected and washed twice with 50 mL of brine solution. Then ether solution was dried over anhydrous MgSO₄. Evaporation of ether followed by distillation at reduced pressure gave the product as a highly viscous yellow oil. This compound was further used for the next step without any purification.

(ii) Pyridacyl pyridinium iodide salt (**B**) was synthesized following the literature procedure.²⁴

(iii) **4-(*N,N*-dimethylamino-phenyl)-(2,2'-bipyridine)**. Pyridacyl pyridinium iodide salt (**B**) (5.2 g, 0.015 mol) was dissolved in 50 mL glacial acetic acid in a 250 mL round bottom flask. To this solution ammonium acetate (12.0 g, 0.13 mol) was added and stirred at 100 °C. Further, 3.0 g (0.015 mol) of 4-(*N,N*-dimethylamino-phenyl)-propanal (**A**) was added to this in three intervals of 1.5 h at 100 °C. This overall reaction mixture was stirred at 100 °C for 16 h. Then the reaction mixture was allowed to cool to room temperature and acetic acid was removed under vacuum. To this about 50 mL of water was added. The pH of this solution was adjusted to ~8.0 and then the desired compound was extracted with chloroform. The chloroform layer was dried over anhydrous MgSO₄ and evaporated to get **L**₂ in its crude form. This was purified by gravity chromatography using silica as the stationary phase and methanol–chloroform (5:95; v/v) as the eluent. Yield: 0.80 g (18%). ES-MS; (**M**⁺): 275 (100%); ¹H NMR (200 MHz CD₃OD; ppm): δ 8.71–8.63 (m, 1H, H_{pyridyl}), 8.42 (d, *J* = 8.0 Hz, 1H, H_{pyridyl}), 7.72 (m, 4H, H_{pyridyl}), 7.27 (d, *J* = 8 Hz, 1H, H_{pyridyl}), 7.33–7.26 (m, 1H, 1H_{pyridyl}), 6.91 (d, *J* = 8 Hz, 1H, H_{phenyl}), 6.85 (d, *J* = 8 Hz, 2H, H_{phenyl}), 3.06 (s, 6H_{methyl}). IR (KBr pellet, cm⁻¹): 1604 (C=C, C=N).

Complex 2. To 50 mL ethanol, 80 mg (0.154 mmol) of Ru(bpy)₂Cl₂·2H₂O and 42 mg (0.154 mmol) of 4-(*N,N*-dimethylamino)-2,2'-bipyridine was added. This reaction mixture was heated to reflux for 8 h. To this an aqueous solution of excess KPF₆ was added and stirred for few minutes. Then ethanol was removed under reduced pressure and an orange solid suspended in water was obtained. This orange solid was then filtered and washed with cold water and ether. Column chromatographic purification,

using alumina as the stationary phase and acetonitrile as the eluent, afforded the desired complex as a dark orange solid. Yield: 30%; MS (ESI-MS) *m/z*: 834 (**M**⁺ – PF₆); ¹H NMR (200 MHz, CD₃CN, ppm): δ 8.66 (2H, d, *J* = 7 Hz, 2H_{L2 5,6}); 8.51 (5H, d, *J* = 8.2, H_{bpy 3,3'}, H_{L3'}); 8.09–8.01 (6H, m, H_{bpy 6,6'}, H_{L2,6,6'}); 7.79–7.72 (7H, m, H_{bpy 4,4'}, H_{phenyl}, H_{L2}); 7.42–7.36 (5H, m, H_{bpy 5,5'}, H_{L2,5'}); 6.85 (2H, d, *J* = 9 Hz, H_{phenyl}); 3.04 (6H, s, H_{L2CH3}). IR (KBr pellet, cm⁻¹): 847 (–PF₆). Calculated for RuC₃₈H₃₃N₇P₂F₁₂: C 46.63, H 3.40, N 10.02; Found: C 46.5; H 3.38; N 9.98. *E*_{1/2} (in CH₃CN): 1.25 (Ru²⁺/Ru³⁺); –1.21 (L₁/L₁[–]) vs. Ag/AgCl.

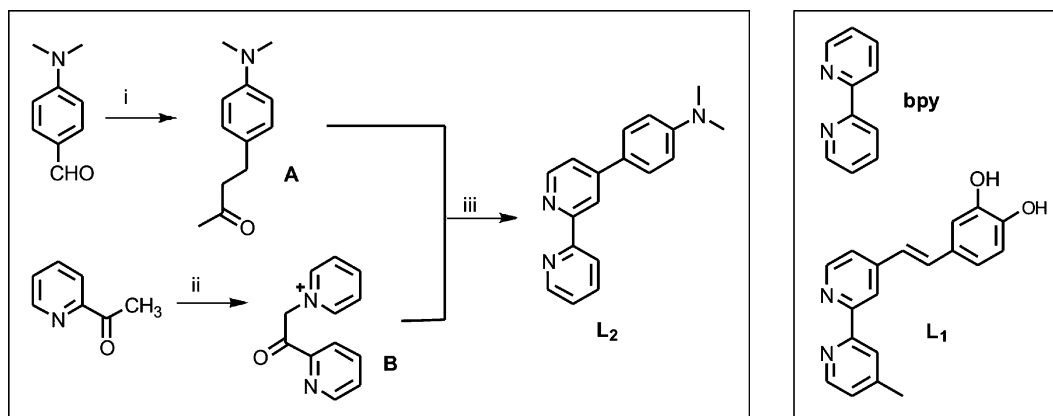
Complex 3. To 30 mL DMF, 75 mg (0.282 mmol) of RuCl₃·3H₂O and 45 mg (0.282 mmol) of 2,2'-bipy was added. After stirring in the dark for 2 h at 90 °C and maintaining an Ar atmosphere, 85 mg (0.282 mmol) of 4-[2-(4'-methyl-2,2'-bipyridinyl-4-yl)vinyl] benzene-1,2-diol (**L**₁) was added at 120 °C and stirred for 4 h. 77.5 mg (0.282 mmol) of 4-(2,2'-bipyridin-4-yl)-*N,N*-dimethylaniline (**L**₂) was added to this reaction mixture and was heated to 145 °C for 4 h more. After evaporation of DMF under reduced pressure, aqueous solution of excess KPF₆ was added and sonicated for 5 min. An orange solid was precipitated and collected by filtration after repeated washing with cold water and ether. Chromatographic purification of the desired compound, using alumina as the stationary phase and acetonitrile as the eluent, afforded the desired complex as a dark orange solid. Yield: 30%; Calculated for RuC₄₇H₄₁N₇O₂P₂F₁₂: C 50.6, H 3.67, N 8.7; Found: C 51.0, H 3.7, N 8.51; MS (ESI-MS) *m/z*: 837 (**M**⁺ – 2PF₆); ¹H NMR (200 MHz, CD₃CN, ppm): δ 9.68 (H, s, H_{3L3}); 8.65 (2H, d, *J* = 7 Hz, 2H_{bpy 6,6'}); 8.49 (3H, d, *J* = 8.2, H_{L2 3',6'}, H_{L2 3'}); 8.05 (4H, t, *J* = 7.4 Hz, H_{L2 4'5'}, H_{bpy 4,4'}); 7.81–7.66 (9H, m, H_{bpy 5,5'}, H_{ethenyl}, H_{L1 5'}, H_{L26}, H_{phenyl 5,6}, H_{L2 3,5}); 7.55 (2H, s, H_{L1 3}), 7.29–7.23 (4H, m, H_{bpy 3,3'}, H_{L2 5',6'}); 6.85 (2H, d, *J* = 9 Hz, H_{L2 2,6}); 6.76 (3H, d, *J* = 9 Hz, H_{ethenyl}, H_{L1 5}, H_{L2 6}); 3.04 (6H, s, H_{L2 CH3}); 3.03 (3H, s, H_{L1 CH3}); IR (KBr pellet, cm⁻¹): 3435 (–OH), 847 (–PF₆). *E*_{1/2} (in CH₃CN): 1.24 (Ru²⁺/Ru³⁺); –1.22 (L₁/L₁[–]) vs. Ag/AgCl.

d) Picosecond time-resolved fluorimeter. Time-resolved fluorescence measurements were carried out using a diode laser based spectrofluorometer from IBH (UK). The instrument works on the principle of time-correlated single-photon counting (TCSPC).²⁵ In the present work, a 406 nm (FWHM ~ 66 ps, 1 MHz) diode laser was used as the excitation light sources, and a TBX4 detection module (IBH) coupled with a special Hamamatsu PMT was used for fluorescence detection.

3. Results and discussion

(a) Synthesis

Pyridacyl pyridinium iodide salt (**B**) and 4-(*N,N'*-dimethylamino-phenyl)-propanal (**A**) were allowed to react for the synthesis of **L**₂ following the basic synthetic methodology reported earlier.^{23d} The synthesis of ligand **L**₁ is reported earlier.^{23a,b} Complex **2** was synthesized following the typical procedure by reacting Ru(bpy)₂Cl₂ with **L**₂ in ethanol and was isolated as the hexafluorophosphate salt. Complex **3** was synthesized following a one pot synthesis, where RuCl₃·3H₂O was initially reacted with one equivalent of 2,2'-bipyridine at 90 °C in DMF solution. To this resulting mixture, **L**₁ was added and allowed to react with Ru(bpy)Cl₃ produced *in situ*, and the reaction temperature was raised to 120 °C. To this resulting



Scheme 2 i: CH_3CHO , EtOH, 28% NaOH, 0°C ; ii: Py, L_2 , reflux, 90 min, N_2 atmp. iii: CH_3COOH , $\text{CH}_3\text{COO}^-\text{NH}_4^+$.

reaction mixture that contains $\text{Ru}(\text{bpy})\text{L}_1$, L_2 was added and the temperature was raised to 145°C . At the end of the reaction, DMF was removed under reduced pressure and the crude product was further purified by column chromatography to achieve the desired purity. Analytical and spectroscopic data obtained for complexes **2** and **3**, agreed well with the proposed structure for the respective complexes.

b) Cyclic voltammetry

Electrochemical studies revealed that the $\text{Ru}^{\text{II/III}}$ redox potential (with respect to Ag/AgCl) for complexes **1**, **2** and **3** is $+1.32\text{ V}$, $+1.25\text{ V}$ and $+1.24\text{ V}$, respectively. This difference in the $\text{Ru}^{\text{II/III}}$ redox potential is reflected in the observed redshift of the MLCT band for complex **3** as compared to the heteroleptic complex **1**.

(c) Spectroscopic properties: UV-vis absorption spectra

The optical absorption spectra of complexes **1**, **2** and **3** were measured at the same concentration in acetonitrile and presented in Fig. 1. Electronic spectra recorded for L_1 (Fig. S3a, ESI[†]) revealed a prominent $\pi\text{-}\pi^*$ transition at 336 nm , along with an $n\text{-}\pi^*$ transition at an even shorter wavelength. Presumably this absorption band moves to about 351 nm in complex **1**. However, our earlier studies suggest that the absorption band in this region ($348\text{--}351\text{ nm}$) is predominantly due to intra-ligand (bpy or L_1) or inter-ligand ($\text{L}_1\text{[}\pi\text{]}-\text{bpy}[\pi^*]$)-based transitions.^{23c} The transition at 351 nm has some contribution from the $d\pi_{\text{Ru(II)}} \rightarrow \pi^*_{\text{L}_1}$ -based MLCT transition; while the transition band with a maxima at 457 nm is predominantly a $d\pi_{\text{Ru(II)}} \rightarrow \pi^*_{\text{L}_1/\text{bpy}}$ -based MLCT transition. Such a $d\pi_{\text{Ru(II)}} \rightarrow \pi^*_{\text{L}_1/\text{bpy}}$ -based MLCT transition band at $\sim 457\text{ nm}$ has been observed earlier by many researchers for various $\text{Ru}(\text{II})$ -polypyridyl complexes.^{23f} No appreciable change in the electronic spectra for complex **1** is observed on addition of HNO_3 ($\text{pH} \sim 1$) as this acidity is not sufficient for protonation of the hydroxyl functionality of the pendant catechol moiety.

The absorption spectra recorded for L_2 (Fig. S3b, ESI[†]) reveals that the tail of the absorption band with a maxima at 336 nm extends beyond 500 nm . An absorption band at 336 nm was assigned to the $\pi\text{-}\pi^*$ -based transition, while the weaker absorption having a tail beyond 500 nm can be assigned to intramolecular

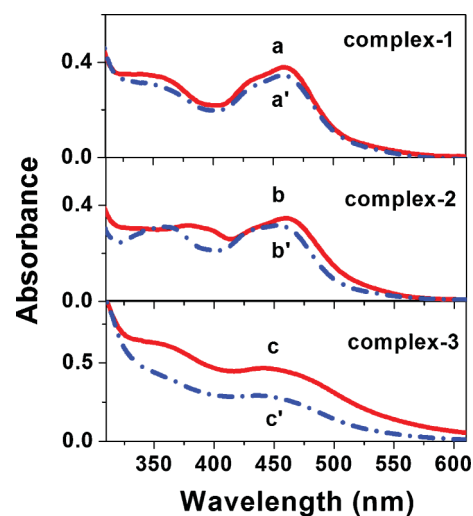


Fig. 1 Optical absorbance spectra of (a) complex **1**, (b) complex **2** and (c) complex **3** in neutral (bold lines) and (a') complex **1**, (b') complex **2** and (c') complex **3** in acidic (dash-dot lines) conditions in acetonitrile (concentrations of all complex were kept the same).

charge transfer transitions. The MLCT electronic transitions for complex **2** are expected to be somewhat similar to that of complex **1**. Thus, the broader absorption ($\lambda > 350\text{ nm}$) represents overlapped MLCT and ILCT electronic transitions. Earlier, Zhang and coworkers²² reported the presence of an ILCT electronic transition in related $\text{Ru}(\text{II})$ -polypyridyl complexes which comprise $-\text{NMe}_2$ groups as electron donating units on diimine ligands. In this present study, the ILCT states are evidenced in complex **2** by a decrease in optical density after protonation (Fig. 1b'). In the presence of HNO_3 , an ILCT transition is expected to be eliminated after protonation of the $-\text{N}_{\text{NMe}_2}$ -centre ($-\text{NH}^+_{\text{NMe}_2}$ formation) and is perhaps reflected by the decrease in the absorbance in the $350\text{--}410\text{ nm}$ region. On the contrary, the protonation of the $-\text{N}_{\text{NMe}_2}$ -centre ($-\text{NH}^+_{\text{NMe}_2}$ formation) is also expected to lower the L_2 -based LUMO energy level and thus with the narrower HOMO-LUMO gap, the $d\pi_{\text{Ru(II)}} \rightarrow \pi^*_{\text{L}_2/\text{bpy}}$ -based MLCT transition is expected to shift to the longer wavelength. Thus, the observed absorption spectra for the protonated complex **2** in the $410\text{--}600\text{ nm}$ region is the result of two opposing influences (Fig. 1b'). The spectral

change in the 350–400 nm region and the slight decrease in the overall optical density (350–550 nm region) after protonation of complex **2** signifies the presence of an ILCT electronic transition in the neutral complex **2**.

However, the broad absorption spectrum of complex **3** (Fig. 1c) is a little more affected by the L_1 and L_2 ligand's electronic properties. The presence of the $-NMe_2$ functionality in L_2 and the extended conjugated system in the catechol-based bpy derivative (L_1) are expected to favour the interligand charge transfer transitions. Earlier, Chi, Chou and their co-workers⁸ have reported LLCT transitions in osmium–polypyridyl complexes containing both electron donor and acceptor ligands. The combination of MLCT and LLCT absorption bands was responsible for the broad absorption spectrum in the longer wavelength region. In the case of complex **3**, the HOMO–LUMO energy gap for this $\pi_{L_2}(\text{HOMO}) \rightarrow \pi^*_{L_1}$ -based transition is expected to be narrower than expected for a $\pi_{L_2}(\text{HOMO}) \rightarrow \pi^*_{\text{bpy}}$ -based transition in complex **2** and accounts for the longer wavelength absorbance with the tail extending to ~ 575 nm (Fig. 1c). This interligand $\pi_{L_2}(\text{HOMO}) \rightarrow \pi^*_{L_1}$ -based transition is affected significantly in acidic solution (pH ~ 1) due to the protonation of the $-NMe_2$ functionality in L_2 ligand; while this is expected to shift the $d\pi_{\text{Ru(II)}} \rightarrow \pi^*_{L_2/\text{bpy}}$ -based MLCT transition to longer wavelength (Fig. 1c'). The protonation of the $-NMe_2$ group suppresses the electron donor character of the L_2 ligand which inhibits the interligand electron transfer processes, a condition essential for the LLCT excited state.²⁶ Thus, the significant decrease in the absorption band on protonation of complex **3** indicates a strong contribution of LLCT electronic transition in the neutral complex **3**. However, unambiguous assignment of the ligand localized CT bands in the steady state absorption spectra is difficult due to the presence of various overlapping spectral bands. So, emission spectroscopy is used to develop a better insight of ligand localized CT states.

d) Steady state emission spectroscopy of complexes **1**, **2** and **3**

The photoluminescence spectra of ruthenium(II)–polypyridyl complexes are largely attributed to the $^3\text{MLCT}$ states in the literature which are populated *via* an ultrafast ISC process from directly photoexcited $^1\text{MLCT}$ states.^{17,18} Fig. 2a shows the emission spectra of complex **1** in aerated acetonitrile. The emission peak at 621 nm is assigned to the $^3\text{MLCT} \rightarrow S_0$ transition. The emission quantum yield of the complex **1** is observed to be less ($\phi_1 = 0.023$) with respect to that of $\text{Ru}(\text{bpy})_3(\text{PF}_6)_2$ ($\phi = 0.062$ in acetonitrile at room temperature with $\lambda_{\text{max}}^{\text{emission}} = 611$ nm).^{1,27} It is known in the literature that the catechol moiety forms a hydrogen bonded adduct with the surrounding polar solvent molecules, which favours a non-radiative loss of photoexcitation energy.^{23c} This is further supported by the fact that the emission yield increases two fold in complex **1Me**₂ ($\text{Ru}^{\text{II}}(\text{bpy})_2(\text{bpy}-\text{CH}=\text{CH}-\text{ph}(\text{OMe})_2)$) where the $-\text{OH}$ group is replaced with an $-\text{OMe}$ group in the Me_2L_1 ligand. Thus, the lower emission quantum yield of complex **1** is attributed to non-radiative decay through a H-bonding network of the catechol moiety. Fig. 2b shows the emission spectra of complex **2** in acetonitrile with a maxima at 623 nm. The emission quantum yield 0.016 (ϕ_2) of complex **2** is observed to be lower as compared to that of complex **1** ($\phi_1 = 0.023$). The lower emission quantum yield of complex **2** can be due to the crossing of $^3\text{MLCT}$ states to lower

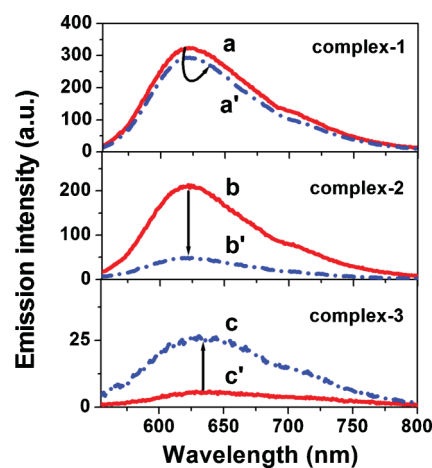
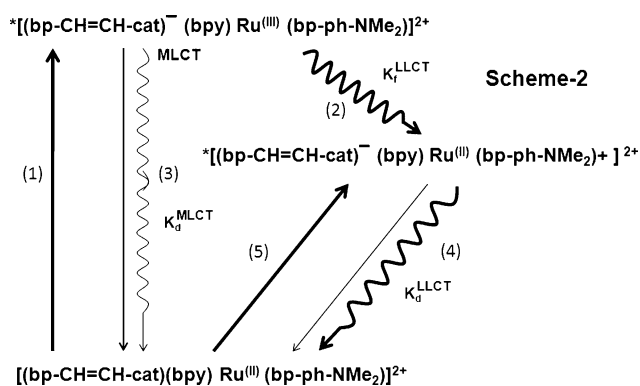


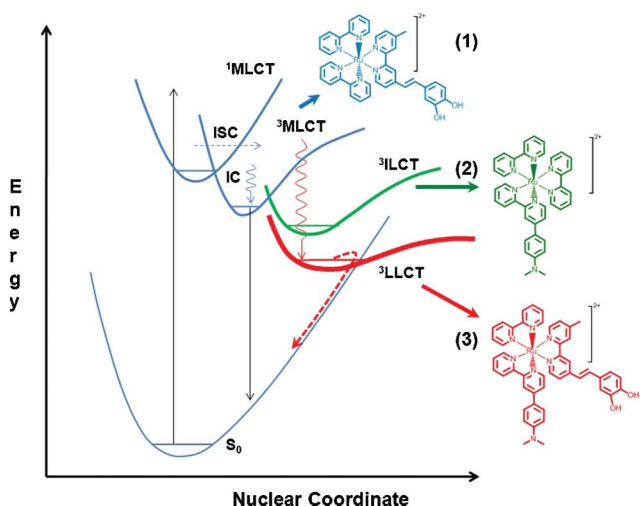
Fig. 2 Emission spectra of (a) complex **1**, (b) complex **2** and (c) complex **3** in neutral (bold lines) conditions and (a') complex **1**, (b') complex **2** and (c') complex **3** in acidic (dash-dot lines) conditions in acetonitrile (all emission spectra are normalized with respect to the same optical density).

energetic $^3\text{ILCT}$ excited states. Earlier, the low emissive behaviour of the ILCT state has been suggested by Charlot and co-workers²⁸ by considering the absence of heavy atom spin density on the $^3\text{ILCT}$ state which decreases the radiative transition from $^3\text{ILCT}$ states in comparison to $^3\text{MLCT}$ states. The low emission quantum yield of the structurally related $\text{Ru}(\text{II})$ –polypyridyl complex was reported by Zhang and co-workers and attributed to ILCT states.²² Thus, the presence of $^3\text{ILCT}$ excited states could be the reason of observing low emission yield for complex **2**. On addition of HNO_3 (excess H^+ ions), the emission yield of complex **2** is further reduced by a factor of ~ 2.9 (Fig. 2b'). The drastic reduction in the emission quantum yield is possibly due to increase in non-radiative decay on protonation of the NMe_2 group of L_2 ligand. This also indicates a weak ILCT character in complex **2**.

Fig. 2c shows the emission spectra of complex **3** in acetonitrile. The emission maximum of complex **3** is observed to be redshifted at 640 nm as compared to emission maxima of complex **1** and **2**. The emission quantum yield of complex **3** ($\phi_3 = 0.0006$) is observed to be extremely low as compared to that of complex **1** ($\phi_1 = 0.023$) and complex **2** ($\phi_2 = 0.016$) and this cannot be explained alone by the non-radiative decay channel caused by the H-bonding network of the catechol moiety as observed in complex **1** or $^3\text{ILCT}$ state as observed in complex **2**. This can be attributed to the $^3\text{LLCT}$ states which are suggested by large redshifted absorption spectra of complex **3** (Fig. 1c). The extremely low emission quantum yield of complex **3** suggests a very low lying LLCT state (energy gap law²⁹) as compared to the $^3\text{MLCT}$ manifold. In this regard, Chi, Chou and coworkers¹⁶ have suggested shallow potential energy surfaces of low lying $^3\text{LLCT}$ excited states (T_1) which under extreme conditions of surface crossing between T_1 and S_0 states (Scheme 4) can yield an extremely low emission yield on account of the thermally activated vibrational states near the crossing point.³⁰ Also, McCusker and co-workers¹⁴ have reported the excited state (ES) vibronic coupling to ground states (S_0) and observed a low emission yield of a Ru^{II} complex on account of intra-ligand electron delocalization. So, the extremely low emission quantum yield of complex **3** in comparison to that of complex **1** and **2** can be assigned to strong LLCT character of complex **3**. Interestingly,



Scheme 3 Straight arrows (1) and (5) represent direct $S_0 \rightarrow$ MLCT and $S_0 \rightarrow$ LLCT transitions; curved arrows (2), (3) and (4) indicate radiationless transitions; bold arrows indicates dominant photo processes.



Scheme 4 A simplified pictorial representation of different photophysical processes in complex **1** (blue), **2** (green) and **3** (red) (Common ground state (S_0), 1 MLCT and 3 MLCT states are shown for the sake of convenience only).

on addition of HNO_3 (excess H^+ ion), the emission yield increases by a factor of four (Fig. 2c'). In acidic conditions (acetonitrile– HNO_3), the protonation of the NMe_2 moiety of the L_2 ligand suppresses the electron donor character of the L_2 ligand which in turn suppresses the strong LLCT character of complex **3**. Therefore, we observed an increased emission yield of protonated complex **3**. This indicates strong LLCT character in complex **3**. Furthermore, the emission yield of protonated complex **2** and complex **3** are observed to be of same order. This suggests that the observed emission of complex **2** and complex **3** in acidic conditions is purely due to the 3 MLCT state.

e) Steady state emission studies at low temperature (77 K)

The ligand localized CT states (ILCT or LLCT) emission is too low to observe in emission spectroscopy at room temperature. The ligand localized excited states are lower in energy as compared to 3 MLCT states. As a result, the vibrational coupling to the ground state is relatively high for ligand localized CT states. So, the low emissive behaviour of ligand localized CT states can be due to thermally activated non-radiative decay processes associated with

ILCT or LLCT excited states. The emission measurements are carried out at 77 K in an ethanol–methanol mixture (4:1 v/v). Fig. 3 shows the uncorrected emission spectra of complex **1**, **2** and **3** at 77 K. The emission spectral feature of complex **1**, **2** and **3** in the 570–670 nm region are observed to be same as that of $\text{Ru}(\text{bpy})_3$ complex reported by Balzani and co-workers.³⁸ The spectral features in this region (570–670 nm) can be assigned to vibronic progression in the 3 MLCT states. Unlike the emission spectra observed at room temperature, the emission intensity of complex **3** is observed to be comparable to that of complex **1** and **2** at 77 K. Interestingly, complexes **2** and **3** exhibit a new emission band in the 670–760 nm region. The new redshifted emission band in 670–750 nm region is attributed to the ILCT excited states of complex **2** and LLCT excited states of complex **3**. The emission spectra are measured at 77 K and presented in the ESI (Fig. S10†). The lifetime of the ILCT and LLCT states are observed to be $\sim 9 \mu\text{s}$ and $\sim 22 \mu\text{s}$, respectively.

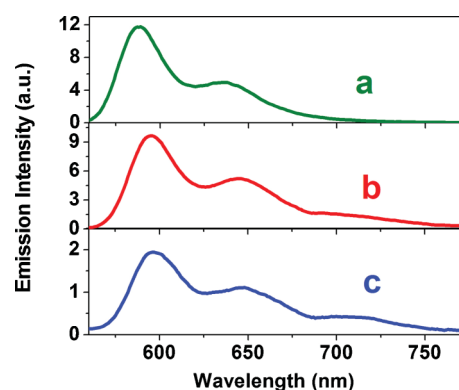


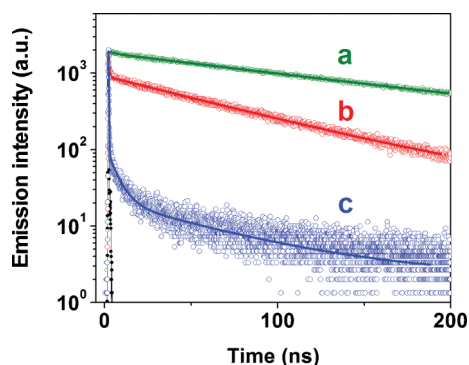
Fig. 3 Uncorrected emission spectra of (a) complex **1**, (b) complex **2** and (c) complex **3** at 77 K in an ethanol–methanol mixture (v/v 4:1).

f) Time resolved emission (TCSPC) studies of complexes **1**, **2** and **3**

The photophysical properties of ruthenium–polypyridyl complexes are largely dominated by MLCT transitions. On photoexcitation in the visible region, a directly populated 1 MLCT excited state undergoes an ultrafast ISC process and 3 MLCT excited states are formed with almost unit quantum yield.^{17,18} The lifetime of 3 MLCT excited states are reported in the sub-microsecond domain.^{29b} Fig. 4a shows the emission decay kinetics of complex **1** at 621 nm ($\lambda_{\text{max}}^{\text{emission}}$) monitoring wavelength in aerated acetonitrile using 406 nm laser pulse (FWHM ~ 66 ps) photoexcitation. The decay kinetics are best fitted bi-exponentially with time constants of 3.6 ns (7%) and 150 ns (93%) (Table 1). Similar, bi-exponential decay profiles have been reported in our earlier studies on related $\text{Ru}(\text{II})$ and $\text{Os}(\text{II})$ –polypyridyl complexes *viz* the $\text{Os}(\text{II})(\text{bpy})_2(\text{L}_1)$ complex.³² The longer component (~ 150 ns) is attributed to a $\pi^*_{(\text{bpy})} \rightarrow d_{\text{Ru}(\text{II})}$ -based 3 MLCT transition as it matches well with the emission decay kinetics of a $\text{Ru}(\text{II})(\text{bpy})_3$ complex in aerated solution (Fig. S9a, ESI†). The non-radiative behaviour of $\pi^*_{\text{L}_1} \rightarrow d_{\text{Ru}(\text{II})}$ transitions, observed previously in steady state emission measurements, is attributed to the shorter decay component (3.6 ns). The bi-exponential decay process in complex **1** is reconfirmed in de-aerated conditions (Fig. S8b, ESI†) where emission kinetics are best fitted with 6 ns (6%) and >315 ns (94%) time constants. Fig. 4b shows the emission decay kinetics of

Table 1 Time resolved emission kinetics data of complex **1**, **2** and **3** in different conditions

$\lambda_{\text{ex}} = 406 \text{ nm}$	Complex 1 ($\lambda_{\text{em}} = 621 \text{ nm}$)	Complex 2 ($\lambda_{\text{em}} = 623 \text{ nm}$)	Complex 3 ($\lambda_{\text{em}} = 640 \text{ nm}$)
Neutral Acetonitrile Air (O ₂)	3.6 ns (7%) 150 ns (93%)	700 ps (47%) 80 ns (53%)	200 ps (97%) 3.5 ns (2%) 74 ns (1%)
Neutral Acetonitrile Inert (N ₂)	6 ns (6%) 315 ns (94%)	700 ps (45%) >300 ns (55%)	200 ps (96%) 3.2 ns (3.2%) >500 ns (1.8%)
Acidic (HNO ₃) Acetonitrile Air (O ₂)	4.2 ns (14%) 150 ns (86%)	380 ps (85%) 6 ns (7.4%) 140 ns (7.6%)	340 ps (87%) 3.7 ns (8%) 140 ns (5%)

**Fig. 4** Emission decay kinetics of (a) complex **1**, (b) complex **2** and (c) complex **3** at respective emission peak wavelengths in aerated conditions. ($\lambda_{\text{ex}} = 406 \text{ nm}$; laser source $\sim 66 \text{ ps}$ FWHM).

complex **2** in aerated acetonitrile monitored at 623 nm ($\lambda_{\text{max}}^{\text{emission}}$). The emission decay kinetics is bi-exponentially fitted with time constants of 700 ps (47%) and 80 ns (53%) (Table 1). Similar bi-exponential decay kinetics (700 ps (45%) and >300 ns (55%), Table 1) is observed in de-aerated conditions (Fig. S8, ESI†) which rule out ³MLCT state quenching by dissolved O₂ in acetonitrile as reported in the literature.¹⁵ Furthermore, this emission decay profile is not observed in a 1:1 physical mixture of Ru(bpy)₃ and L₂ molecular entity (Fig. S9c, ESI†). This indicates that the shortest time component (700 ps) is associated with the inherent photophysical process of complex **2**. In complex **2**, the presence of a strong electron donating *N,N'*-dimethylaminophenyl moiety on the bpy ligand (L₂) introduces energetically lower lying ³ILCT excited states (supported by low temperature emission spectra) to ³MLCT states manifold. This can cause significant emission quenching of ³MLCT states *via* internal conversion to ³ILCT excited states (Scheme 4).³¹ Earlier, the ³MLCT → ³ILCT internal conversion is reported to be as fast as $\sim 100 \text{ ps}$ by Charlot *et al.*²⁸ So, in this present study, the 700 ps component can be assigned to ³MLCT → ³ILCT internal conversion process. The longer time component (80 ns in aerated conditions or >300 ns in de-aerated conditions) is associated with remaining ³MLCT excited states. The longer lifetime component of de-aerated sample (>300 ns) may not be accurate due to instrumental limitations of the 500 ns time scale imposed by the 1 MHz repetition rate of the 406 nm laser excitation source. Further, the lifetime of the populated ³ILCT states may not be observed in TCSPC measurements either due to their longer lifetime (reported in the > microsecond time

domain³⁹) or due to the radiationless decay nature of the ³ILCT states. Fig. 4c shows the emission decay profile of complex **3** in aerated acetonitrile at 640 nm monitoring wavelength. The decay profile is best fitted with 200 ps (97%), 3.5 ns (2%) and 74 ns (1%) time constants (Table 1). Similar decay kinetics are observed in de-aerated conditions (Fig. S8c, ESI†) and best fitted with 200 ps (95%), 3.2 ns (3.2%) and >500 ns (1.8%) time constants (Table 1). Such a short component (200 ps) and its large amplitude ($\sim 97\%$) are not observed in complex **1**, complex **2** and the 1:1:1 physical mixture of Ru^{II}(bpy)₃, L₁ and L₂ molecular entities (Fig. S9d, ESI†). In the case of complex **3**, the collective effect of electron donor L₂ ligand and electron acceptor L₁ ligand introduces energetically lower lying ³LLCT excited states (supported by low temperature emission measurements) to ³MLCT manifolds. The lower energetics ³LLCT can significantly quench the ³MLCT state of complex **3**. Earlier, the crossing from ³MLCT to lower energetic ³LLCT excited state are reported to be as fast as <30 ps.³³ So, the shortest component (200 ps) of complex **3** in acetonitrile solvent can reasonably be attributed to ³MLCT → ³LLCT internal conversion. The second and third time components (3.5 ns and 74 ns in aerated conditions) are too low (total 3%) to assign properly. Earlier, Yeh *et al.*³⁶ have shown a ³ILCT → ³LLCT conversion time as 4.9 ns. So, a 3.5 ns time constant can either be associated with ³ILCT → ³LLCT conversion or related with ³MLCT states of the L₁ ligand ($\pi^*_{(\text{bp-CH}=\text{CH-catechol})} \rightarrow d_{\text{Ru(II)}}$ process). The longer component (74 ns in aerated condition or >500 ns in de-aerated conditions) can be assigned to ³MLCT excited states.

The physical interpretation of the ³MLCT → ³LLCT internal conversion process in complex **3** can be given by the intramolecular electron transfer process as depicted in Scheme 3. In the photoexcited ³MLCT state of complex **3**, the presence of the strong oxidant Ru^(III) ion helps in removing an electron from the bp-ph-NMe₂ moiety of the L₂ ligand and produces interligand (between L₁ and L₂ ligand) charge separated excited states (LLCT states). This behavior is supported by earlier studies^{1,34} in reductive quenching of ³MLCT states of $^*[(\text{bpy})^-\text{Ru}^{\text{(III)}}(\text{bpy})_2]^{2+}$ complexes in presence of triethylamine or *N,N'*-dimethylaniline. So, ³MLCT → ³LLCT internal conversion can be interpreted as an intramolecular electron transfer reaction^{5,35} Furthermore, the photoexcitation through strong LLCT absorption bands of complex **3** can directly populate the interligand charge separated excited states (LLCT state) as depicted in Scheme 3.

g) Time resolved emission studies (TCSPC) of complexes **1**, **2** and **3** at low pH

Steady state emission measurements of complex **1**, **2** and **3** in the presence of excess H⁺ ions revealed suppression of ligand localized CT states due to protonation of the *N,N'*-dimethylaminophenyl moiety of L₂ ligand in complex **2** and **3**. So, the time resolved emission studies (TCSPC) are carried out in acidic conditions (adding HNO₃ in acetonitrile) to understand the ³MLCT excited state conversion to ligand localized CT states (ILCT in complex **2** and LLCT in complex **3**). Fig. 5a shows the decay profile of complex **1** in the presence of excess of H⁺ ions which is best fitted with time constants of 4.2 ns (14%) and 150 ns (86%) (Table 1). The decay kinetics of complex **1** in acidic conditions is observed to be similar to that in neutral conditions (Fig. 4a). The slight increase of

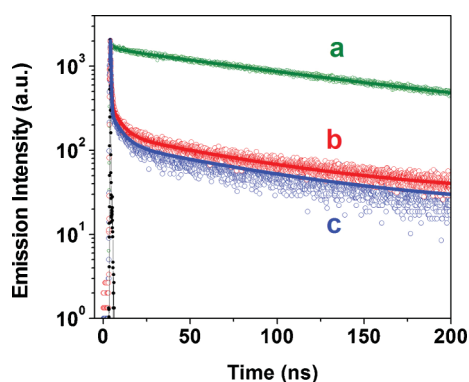


Fig. 5 Emission decay kinetics of protonated (a) complex 1, (b) complex 2 and (c) complex 3 at respective emission peak wavelengths in aerated conditions ($\lambda_{\text{ex}} = 406$ nm; laser source ~ 66 ps FWHM).

first component (14%) can be attributed to a decrease in its $^3\text{MLCT}$ energy level (L_1 ligand) which populates more from $^3\text{MLCT}$ states involving bpy ligand as per the energy gap law.³⁷ Fig. 5b shows the emission decay profile of protonated complex 2 and best fitted with multi-exponential time constants of 380 ps (85%), 6 ns (7.4%) and 140 ns (7.6%) (Table 1). A similar decay profile is observed for complex 3 (Fig. 5c) which is multi-exponentially fitted with time constants of 340 ps (87%), 3.7 ns (8%) and 140 ns (5%) (Table 1). It is interesting to observe a similar emission decay profile for complex 2 and complex 3 (Fig. 5) in acidic conditions in contrary to their widely different emission decay profile of non-protonated complex 2, complex 3 (Fig. 4) and 1:1:1 physical mixture of $\text{Ru}^{\text{II}}(\text{bpy})_3$, L_1 and L_2 molecular species (Fig. S9d, ESI[†]). The ligand localized CT excited states of complex 2 and complex 3 are different in nature (ILCT vs. LLCT) and also different in energetics (LLCT lower energetic than ILCT excited state). As a result the internal conversion process in two complexes occurs with different timescales (700 ps vs. 200 ps in Fig. 4b and 4c) and with different strength (45% vs. 96% in Fig. 4b and 4c). In acidic conditions, the ligand localized CT states are suppressed and two complexes exhibit similar decay kinetics in TCSPC measurements. The lower emission yield of complex 2 in acidic conditions as compared to that in neutral conditions (Fig. 2b and 2b'), suggests the initiation of a new non-radiative decay process due to the protonated NMe_2 moiety of the L_2 ligand. Therefore, the 360 ± 20 ps time constant is assigned to the decay of the $^3\text{MLCT}$ state due to a non-radiative process in the protonated complex 2 and 3.

4. Conclusions

We have synthesized ruthenium(II) diimine complexes (1) $\text{Ru}(\text{II})(\text{bpy})_2(\text{L}_1)$, (2) $\text{Ru}(\text{II})(\text{bpy})_2(\text{L}_2)$ and (3) $\text{Ru}(\text{II})(\text{bpy})(\text{L}_1)(\text{L}_2)$, where $\text{bpy} = 2,2'$ -bipyridyl, $\text{L}_1 = 4$ -[2-(4'-methyl-2,2'-bipyridinyl-4-yl)vinyl]benzene-1,2-diol and $\text{L}_2 = 4$ -(*N,N*-dimethylamino-phenyl)-(2,2'-bipyridine) and investigated the ligand localized charge transfer (ILCT and LLCT) states using optical absorption and emission studies. The experimental measurements were carried out in different conditions like aerated vs. de-aerated, protonated vs. de-protonated and ambient vs. low temperature. In complex 3, the presence of electron donating L_2 ligand and electron withdrawing L_1 ligand introduces new low energetic LLCT excited states to MLCT manifolds. The optical absorption

spectrum of complex 3 is redshifted and broadened in comparison to that of complex 1 and 2 on account of the superimposed LLCT and MLCT states in the 350–700 nm region. The extremely low emission quantum yield of complex 3 is attributed to the quenching of $^3\text{MLCT}$ states by the lower energetic $^3\text{LLCT}$ states which are low-emissive at room temperature. The ligand localized CT state (ILCT and LLCT) emission of complex 2 and 3 are revealed by the appearance of a new luminescence band in the 670–760 nm region at 77 K. On photoexcitation of complex 3, the LLCT excited state is populated directly *via* the LLCT absorption band (350–700 nm) or indirectly through internal conversion from photoexcited $^3\text{MLCT}$ (400–600 nm). The internal conversion process is studied by quenching of $^3\text{MLCT}$ emission using time resolved emission studies. The internal conversion to ILCT and LLCT excited states are observed to be as fast as ~ 700 ps and ~ 200 ps time scale in complex 2 and 3, respectively. This study helps to understand the effect of ligand localized excited state on the photophysical property of heteroleptic ruthenium(II) polypyridyl complexes.

Acknowledgements

We thank Dr T. Mukherjee and Dr S. K. Sarkar of BARC and Dr P. K. Ghosh of CSMCRI for their constant encouragement. HNG thanks BRNS while AD thanks DST and BRNS for financial assistance. We also like to thank Prof. Anindya Dutta of IIT, Mumbai and Dr V. Sudarsan of Chemistry Division, BARC for their kind help in recording time-resolved photoluminescence kinetics.

References

- 1 A. Juris, V. Balzani, F. Barigelletti, S. Campagna, P. Belser and A. von Zelewsky, *Coord. Chem. Rev.*, 1988, **84**, 85.
- 2 (a) M. Maestri, N. Armaroli, V. Balzani, E. C. Constable and A. M. W. C. Thompson, *Inorg. Chem.*, 1995, **34**, 2759; (b) K. Kalyanasundaram and M. Grätzel, *Coord. Chem. Rev.*, 1998, **177**, 347.
- 3 K. Kalyanasundaram, *Coord. Chem. Rev.*, 1982, **46**, 159.
- 4 (a) A. Vogler and H. Kunkely, *Comments Inorg. Chem.*, 1990, **9**, 201; (b) S. I. Gorelsky, E. S. Dodsworth, A. B. P. Lever and A. A. Vlcek, *Coord. Chem. Rev.*, 1998, **174**, 469.
- 5 (a) T. A. Perkins, D. B. Pourreau, T. L. Netze and K. S. Schanze, *J. Phys. Chem.*, 1989, **93**, 4511; (b) Y. Wang, B. T. Hauser, M. M. Rooney, R. D. Burton and K. S. Schanze, *J. Am. Chem. Soc.*, 1993, **115**, 5675.
- 6 (a) B. O'Regan and M. Grätzel, *Nature*, 1991, **353**, 737.
- 7 (a) M. K. Nazeeruddin, Q. Wang, L. Cevey, V. Aranyos, P. Liska, E. Figgemeier, C. Klein, N. Hirata, S. Koops, S. A. Haque, J. R. Durrant, A. Hagfeldt, A. B. P. Lever and M. Grätzel, *Inorg. Chem.*, 2006, **45**, 787; (b) P. G. Bomben, K. C. D. Robson, P. A. Sedach and C. P. Berlinguette, *Inorg. Chem.*, 2009, **48**, 9631.
- 8 (a) X.-N. Li, Z.-J. Wu, Z.-J. Si, H.-J. Zhang, L. Zhou and X.-J. Liu, *Inorg. Chem.*, 2009, **48**, 7740; (b) Y.-M. Cheng, E. Y. Li, G.-H. Lee, P.-T. Chou, S.-Y. Lin, C.-F. Shu, K.-C. Hwang, Y.-L. Chen, Y.-H. Song and Y. Chi, *Inorg. Chem.*, 2007, **46**, 10276; (c) K.-S. Chen, W.-H. Liu, Y.-H. Wang, C.-H. Lai, P.-T. Chou, G.-H. Lee, K. Chen, H.-Y. Chen, Y. Chi and F.-C. Tung, *Adv. Funct. Mater.*, 2007, **17**, 2964; (d) W. Lu, B.-X. Mi, M. C. W. Chan, Z. Hui, C.-M. Che, N. Zhu and S.-T. Lee, *J. Am. Chem. Soc.*, 2004, **126**, 4958; (e) S. C. Chan, M. C. W. Chan, Y. Wang, C. M. Che, K. K. Cheung and N. Y. Zhu, *Chem.-Eur. J.*, 2001, **7**, 4180.
- 9 (a) C. A. Bignozzi, R. Argazzi and C. J. Kleverlaan, *Chem. Soc. Rev.*, 2000, **29**, 87; (b) M. K. Nazeeruddin, F. D. Angelis, S. Fantacci, A. Selloni, G. Viscardi, P. Liska, S. Ito, B. Takeru and M. Grätzel, *J. Am. Chem. Soc.*, 2005, **127**, 16835; (c) H.-J. Park, K. H. Kim, S. Y. Choi, H.-M. Kim, W. I. Lee, Y. K. Kang and Y. K. Chung, *Inorg. Chem.*, 2010, **49**, 7340.
- 10 X.-N. Li, Z.-J. Wu, H.-J. Zhang, Z.-J. Si, L. Zhou and X.-J. Liu, *Eur. J. Inorg. Chem.*, 2009, **27**, 4052.

- 11 M.-X. Li, X. Zhou, B.-H. Xia, H.-K. Zhang, Q.-J. Pan, T. Liu, H.-G. Fu and C.-C. Sun, *Inorg. Chem.*, 2008, **47**, 2312.
- 12 I. Avilov, P. Minoofar, J. Cornil and L. D. Cola, *J. Am. Chem. Soc.*, 2007, **129**, 8247.
- 13 A. Vlček Jr. and S. Zláliš, *Coord. Chem. Rev.*, 2007, **251**, 258.
- 14 N. H. Damrauer, T. R. Boussie, M. Devenney and J. K. McCusker, *J. Am. Chem. Soc.*, 1997, **119**, 8253.
- 15 S. Ji, W. Wu, W. Wu, P. Song, K. Han, Z. Wang, S. Liu, H. Guod and J. Zhao, *J. Mater. Chem.*, 2010, **20**, 1953.
- 16 (a) Y. Chi and P.-T. Chou, *Chem. Soc. Rev.*, 2007, **36**, 1421; (b) S.-W. Li, Y.-M. Cheng, Y.-S. Yeh, C.-C. Hsu, P.-T. Chou, S.-M. Peng, G.-H. Lee, Y.-L. Tung, P.-C. Wu, Y. Chi, F.-I. Wu and C.-F. Shu, *Chem.-Eur. J.*, 2005, **11**, 6347.
- 17 (a) N. H. Damrauer, G. Cerullo, A. Yeh, T. R. Boussie, C. V. Shank and J. K. McCusker, *Science*, 1997, **275**, 54; (b) A. C. Bhasikuttan, M. Suzuki, S. Nakashima and T. Okada, *J. Am. Chem. Soc.*, 2002, **124**, 8398.
- 18 (a) J. N. Demas and D. G. Taylor, *Inorg. Chem.*, 1979, **18**, 3177; (b) J. N. Demas and A. W. Adamson, *J. Am. Chem. Soc.*, 1971, **93**, 1800 and references therein.
- 19 R. L. Blakley and M. K. DeArmond, *J. Am. Chem. Soc.*, 1987, **109**, 4895.
- 20 (a) Y. Pellegrin, A. Quaranta, P. Dorlet, M.-F. Charlot, W. Leibl and A. Aukauloo, *Chem.-Eur. J.*, 2005, **11**, 3698; (b) J. D. Lewis, L. Bussotti, P. Foggi, R. N. Perutz and J. N. Moore, *J. Phys. Chem. A*, 2002, **106**, 12202.
- 21 Y. Wang and K. S. Schanze, *Chem. Phys.*, 1993, **176**, 305.
- 22 L.-Q. Song, J. Feng, X.-S. Wang, J.-H. Yu, Y.-J. Hou, P.-H. Xie, B.-W. Zhang, J.-F. Xiang, X.-C. Ai and J.-P. Zhang, *Inorg. Chem.*, 2003, **42**, 3393.
- 23 (a) A. D. Shukla and A. Das, *Polyhedron*, 2000, **19**, 2605; (b) A. D. Shukla, B. Whittle, H. C. Bajaj, A. Das and M. D. Ward, *Inorg. Chim. Acta*, 1999, **285**, 89; (c) D. A. Jose, P. Kar, D. Koley, B. Ganguly, W. Thiel, G. Ramakrishna, D. K. Palit, H. N. Ghosh and A. Das, *Inorg. Chem.*, 2007, **46**, 5576; (d) G. Ramakrishna, D. A. Jose, D. K. Kumar, A. Das, D. K. Palit and H. N. Ghosh, *J. Phys. Chem. B*, 2005, **109**, 15445; (e) S. Verma, P. Kar, A. Das, D. K. Palit and H. N. Ghosh, *Chem.-Eur. J.*, 2010, **16**, 611; (f) V. Balzani, A. Juris and M. Venturi, *Chem. Rev.*, 1996, **96**, 759.
- 24 (a) M. A. Hayes, C. Meckel, E. Schatz and M. D. Ward, *J. Chem. Soc., Dalton Trans.*, 1992, 703; (b) A. Das, J. A. McCleverty, M. D. Ward, C. J. Jones and A. M. W. C. Thompson, *Polyhedron*, 1992, **11**, 2119; (c) A. J. Amoroso, A. Das, J. A. McCleverty, M. F. Barigelletti and L. Flamigni, *Inorg. Chim. Acta*, 1994, **226**, 171.
- 25 D. V. O'Connor, D. Phillips, *Time Correlated Single Photon Counting*; Academic Press, New York, 1984.
- 26 X. Han, L.-Z. Wu, G. Si, J. Pan, Q.-Z. Yang, L.-P. Zhang and C.-H. Tung, *Chem.-Eur. J.*, 2007, **13**, 1231.
- 27 (a) B. Durham, J. V. Caspar, J. K. Nagle and T. J. Meyer, *J. Am. Chem. Soc.*, 1982, **104**, 4803; (b) J. M. Calvert, J. V. Caspar, R. A. Binstead, T. D. Westmoreland and T. J. Meyer, *J. Am. Chem. Soc.*, 1982, **104**, 6620; (c) J. V. Caspar and T. J. Meyer, *J. Am. Chem. Soc.*, 1983, **105**, 5583.
- 28 (a) M.-F. Charlot, Y. Pellegrin, A. Quaranta, W. Leibl and A. Aukauloo, *Chem.-Eur. J.*, 2006, **12**, 796; (b) Y. Pellegrin, A. Quaranta, P. Dorlet, M. F. Charlot, W. Leibl and A. Aukauloo, *Chem.-Eur. J.*, 2005, **11**, 3698.
- 29 (a) P. Chen and T. J. Meyer, *Chem. Rev.*, 1998, **98**, 1439; (b) J. V. Caspar and T. J. Meyer, *J. Am. Chem. Soc.*, 1983, **105**, 5583; (c) J. V. Caspar and T. J. Meyer, *Inorg. Chem.*, 1983, **22**, 2444.
- 30 P.-T. Chou and Y. Chi, *Eur. J. Inorg. Chem.*, 2006, **17**, 3319.
- 31 A. C. Benniston, A. Harriman, D. J. Lawrie and A. Mayeux, *Phys. Chem. Chem. Phys.*, 2004, **6**, 51.
- 32 (a) S. Verma, P. Kar, A. Das, D. K. Palit and H. N. Ghosh, *J. Phys. Chem. C*, 2008, **112**, 2918; (b) A. Ghosh, S. Verma, B. Ganguly, H. N. Ghosh and A. Das, *Eur. J. Inorg. Chem.*, 2009, 2496.
- 33 T. A. Perkins, D. B. Pourreau, T. L. Netzel and K. S. Schanze, *J. Phys. Chem.*, 1989, **93**, 4511.
- 34 N. Kitamura, H. -B. Kim, S. Okano and S. Tazuke, *J. Phys. Chem.*, 1989, **93**, 5750.
- 35 J. D. Lewis, L. Bussotti, P. Foggi, R. N. Perutz and J. N. Moore, *J. Phys. Chem. A*, 2002, **106**, 12202.
- 36 Y.-S. Yeh, Y.-M. Cheng, P.-T. Chou, G.-H. Lee, C.-H. Yang, Y. Chi, C.-F. Shu and C.-H. Wang, *ChemPhysChem*, 2006, **7**, 2294.
- 37 (a) S. R. L. Fernando, U. S. M. Maharroof, K. D. Deshayes, T. H. Kinstle and M. Y. Ogawa, *J. Am. Chem. Soc.*, 1996, **118**, 5783; (b) P.-H. Xie, Y.-J. Hou, B.-W. Zhang, Y. Cao, F. Wu, W.-J. Tian and J.-C. Shen, *J. Chem. Soc., Dalton Trans.*, 1999, 4217.
- 38 A. Juris, V. Balzani, P. Belser and A. V. Zelewsky, *Helv. Chim. Acta*, 1981, **64**, 2175.
- 39 K. F. Mongey, J. G. Vos, B. D. MacCraith, C. M. McDonagh, C. Coates and J. McGarvey, *J. Mater. Chem.*, 1997, **7**, 1473.